ELSEVIER

Applied Catalysis B: Environmental 31 (2001) 51–60

APPLIED CATALYSIS B: ENVIRONMENTAL

www.elsevier.com/locate/apcatb

New $Pd/Ce_xZr_{1-x}O_2/Al_2O_3$ three-way catalysts prepared by microemulsion Part 2. In situ analysis of CO oxidation and NO reduction under stoichiometric $CO+NO+O_2$

A. Martínez-Arias [a], M. Fernández-García [a,*], A. Iglesias-Juez [a], A.B. Hungría [a], J.A. Anderson [b], J.C. Conesa [a], J. Soria [a]

[a] *Instituto de Catálisis y Petroleoquímica, CSIC, Campus Cantoblanco, 28049 Madrid, Spain*
[b] *Department of Chemistry, University of Dundee, Dundee DD1 4HN, Scotland, UK*

Received 17 July 2000; received in revised form 29 October 2000; accepted 29 October 2000

Abstract

The light-off behavior for CO oxidation and NO reduction under stoichiometric $CO + NO + O_2$ gas mixtures of a series of palladium catalysts supported on ceria–zirconia, ceria–zirconia/alumina and alumina has been examined by means of catalytic activity tests, and by DRIFTS, XANES and EPR spectroscopies. The results show the promoting effect of the Zr–Ce mixed oxide on both reactions. The extent of promotion depends on the characteristics of the promoter entities present for each catalyst and on the nature of the reaction. As observed in the absence of NO, CO oxidation was mainly enhanced by contact between Pd and 3D aggregated promoter entities, although an inhibiting effect of NO on CO oxidation, attributed to passivation of the interface sites due to formation of oxidized states of Pd, was observed at low temperatures. In contrast, the higher activity for NO reduction over catalysts supported on ceria–zirconia/alumina suggests that most active sites for that reaction involve Pd interacting with dispersed promoter entities.

Keywords: TWC catalysts; CO oxidation; NO reduction; Palladium; Alumina-supported ceria–zirconia; DRIFTS; XANES; EPR

1. Introduction

The removal of NO_x produced during combustion processes of liquid and gaseous fuels is one of the most significant environmental problems. As mentioned in part 1 of this article [1], the elimination of lead and the lowering of sulfur levels in fuels have allowed the development of catalytic converters using Pd-based systems working under stoichiometric conditions due to their excellent oxidation activity at low temperatures for hydrocarbon and CO as well as their high durability. Several strategies such as alloying with base metals or multilayer formulations have been devised in order to improve the performance of Pd-based systems for NOx elimination [2,3]. However, the improvement of Pd catalysts to meet increasingly stringent requirements for NO emission control firstly requires a comprehensive understanding of the NO reduction processes occurring in such systems. Under stoichiometric conditions, this process always implies the dissociation of the N–O bond, a step of critical importance and, in some conditions, possibly the rate limiting step [2–6].

* Corresponding author.

0926-3373/01/$ – see front matter
PII: S0926-3373(00)00264-2

The behavior of ceria-promoted Pd-based three-way catalysts (TWCs) for NO elimination in stoichiometric mixtures depends critically on the properties of the noble metal–ceria interface [2–4]. The mutual influence of both ceria and palladium components produces the (partial) reduction of Pd and the presence of anionic vacancies in the lanthanide oxide. However, a detailed analysis of classical TWCs components reveals a more complex situation by which a passivation (oxidation) of the metal surface layer is produced by the presence of NO and a competition of oxygen-containing molecules (NO/O_2) for the lanthanide anionic vacancies is detected [3,6]. NO competes with O_2 for the oxidation of the CO molecule but also for the re-filling of anionic vacancies, resulting in a complex response of the catalyst to the presence of this molecule in the reactive mixture. In an attempt to analyze this situation for Pd–Ce/Zr catalysts, the activity of a series of Pd-supported catalysts, involving two $Pd/Ce_xZr_{1-x}O_2/Al_2O_3$ complex catalysts and a $Pd/Ce_{0.5}Zr_{0.5}O_2$ reference, has been tested in the $CO + NO + O_2$ reaction. The behavior of these systems under reaction conditions has been explored by infrared spectroscopy (DRIFTS) and X-ray absorption near edge structure (XANES). The analysis of the anionic vacancies role in the presence of the reactive mixture has been carried out using electron paramagnetic resonance (EPR).

2. Experimental

Catalysts were prepared as indicated in Part 1 [1]. They will be referred to as PdZC, Pd33ZCA, Pd10ZCA and PdA, corresponding to supported 1 wt.% Pd samples using zirconia–ceria, 33 and 10 wt.% zirconia–ceria/alumina, and alumina (Condea, $S_{BET} = 200\,m^2\,g^{-1}$), respectively, as supports.

Catalytic tests using a 1% CO + 0.1% NO + 0.45% O_2 (N_2 balance) mixture at $30.000\,h^{-1}$ were performed in a pyrex glass reactor system. Gases were regulated with mass flow controllers and analyzed on line using a Perkin-Elmer 1725X FTIR spectrometer coupled with a multiple reflection transmission cell (Infrared Analysis Inc.). Oxygen concentrations were determined using a paramagnetic analyzer (Servomex 540A). Prior to catalytic testing, in situ calcination at 773 K was performed, followed by cooling in synthetic air and a N_2 purge at room temperature (RT). A characteristic test consisted of increasing the temperature from 298 to 823 K at $5\,K\,min^{-1}$.

DRIFTS analysis of adsorbed species present on the catalyst surface under reaction conditions was carried out using a Perkin-Elmer 1750 FTIR fitted with an MCT detector. Analysis of the NO conversion at the outlet of the IR chamber was performed by chemiluminescence (Thermo Environmental Instruments 42C). The DRIFTS cell (Harrick) was fitted with CaF_2 windows and a heating cartridge that allowed samples to be heated to 773 K. Samples of ca. 80 mg were calcined in situ (as indicated above) and then cooled to 298 K in synthetic air before introducing the reaction mixture and heating at $5\,K\,min^{-1}$ to 673 K, recording one spectrum ($4\,cm^{-1}$ resolution) every 15 K. The gas mixture (1% CO, 0.1% NO, 0.45% O_2, N_2 balance) was prepared using a computer controlled gas-blender with $75\,cm^3\,min^{-1}$ passing through the catalyst bed.

XANES experiments at the Ce L_{III}- and Pd K-edges were performed on line EXAFS-IV of DCI synchrotron at LURE. A Si(3 1 1) (Ce) or Ge(4 0 0) (Pd) double-crystal monochromator was used in conjunction, in the Ce case, with a rejection mirror to minimize the harmonic content of the beam. Transmission experiments were carried out using N_2/O_2 or Ar-filled ionization chambers. The energy scale was simultaneously calibrated by measuring a CeO_2 wafer or Pd foil using a third ionization chamber. Samples were self-supported (absorbance 0.5–2.0) and placed in a controlled-atmosphere cell for treatment. XANES spectra were taken every 15 K for a Pd33CZA sample in the presence of the $CO + NO + O_2$ mixture during a temperature ramp to 623 K at $5\,K\,min^{-1}$. The series obtained was analyzed by using a statistical method called principal factor analysis [7,8]. The analysis assumes that the absorbance in a set of spectra can be mathematically modeled as a linear sum of individual components, called factors, which correspond to each one of the metal species present in a sample, plus noise [9]. To determine the number of individual components, an *F*-test of the variance associated with factor K and the summed variance associated with the pool of noise factors is performed. A factor is accepted as a "pure" species (factor associated with signal and not noise) when the percentage of significance level of the *F*-test, %SL, is lower than a test level set in previous studies at 5% [7,8]. The ratio between the reduced

eigenvalues, $R(r)$, which must approach one for noise factors, are also used in reaching this decision. Once the number of individual components is set, XANES spectra corresponding to individual palladium species and their concentration profiles were generated by an orthogonal rotation (varimax rotation) which should align factors (as close as possible) along the unknown concentration profiles, followed by iterative transformation factor analysis (ITFA). ITFA starts with delta function representations of the concentration profiles located at temperatures predicted by the varimax rotation, which are then subjected to refinement by iteration until error in the resulting concentration profiles is lower than the statistical error extracted from the set of raw spectra [7,8].

EPR spectra were recorded at 77 K with a Bruker ER 200 D spectrometer operating in the X-band and calibrated with a DPPH standard ($g = 2.0036$). Portions of ca. 40 mg. were placed inside a quartz probe cell with greaseless stopcocks. A conventional dynamic high-vacuum line was used for different treatments. In situ pretreated samples (as indicate above) were reduced with 100 Torr of CO at 423 K for 1 h and evacuated for 30 min at the same temperature. After cooling to room temperature, 10 Torr of NO was admitted to the cell, followed by heating of the samples for 1 h at 423 K, then cooling to room temperature and thorough outgassing. Using these pre-conditioned surfaces, oxygen (ca. 70 μmol g^{-1}) adsorption, followed by 30 min outgassing (residual pressure 2×10^{-4} mbar), was performed at 77 K.

3. Results

3.1. Reactivity tests

The CO and NO conversion profiles for the Pd containing catalysts are presented in Fig. 1. Below 400 K, conversion of NO corresponds to adsorption/desorption processes, as calculated from mass balance of the outlet gases. PdA displays very similar light-off temperatures for CO and NO while CO oxidation proceeds at lower temperatures than NO reduction over the ZC-containing catalysts. The temperature difference between both reactions increases with the ZC-content of the catalyst, being about 25, 50 and 150 K, respectively, for the Pd10ZCA, Pd33ZCA and PdZC samples. The onset of CO oxidation over PdZC and Pd33ZCA is close to room temperature (RT) reaching 100% around 380 and 450 K, respectively. Pd10ZCA does not show CO conversion until approximately 350 K, reaching full conversion around 480 K. For NO reduction, a different trend is observed. PdZC shows only slightly higher activity than PdA while a clear promoting effect is observed using the ZCA-supported systems, the activity increasing slightly with ZC content. The best results in terms of N_2 selectivity are observed for Pd33ZCA which exhibits no N_2O yield at $T > 543$ K, while Pd10ZCA and PdZC achieve more or less constant N_2O yields of ca. 50 and 45%, respectively, at $T > 503$ K and PdA shows ca. 80% N_2O yield between 503 and 543 K gradually decreasing at higher temperatures reaching 33% at the end of the run (603 K).

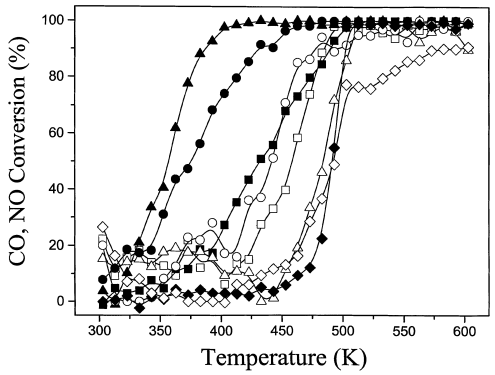

Fig. 1. Conversion profiles of CO (full symbols) and NO (empty symbols) for the CO+NO+O_2 reaction over Pd samples. Triangles: PdZC; circles: Pd33ZCA; squares: Pd10ZCA; rhombus: PdA.

3.2. IR experiments

DRIFT spectra recorded under reaction conditions (Fig. 2A–D) indicate a progressive decrease in CO gas contribution and concomitant increase in the CO_2 production, in rough agreement with the catalytic conversion data (Fig. 1). Although the NO gas contribution is not visible due to its lower concentration and extinction coefficient with respect to CO, the presence of bands in the 2230–2250 cm^{-1} range, characteristic of isocyanate species (NCO) (note that these bands are not formed in the absence of NO [1]), indicates

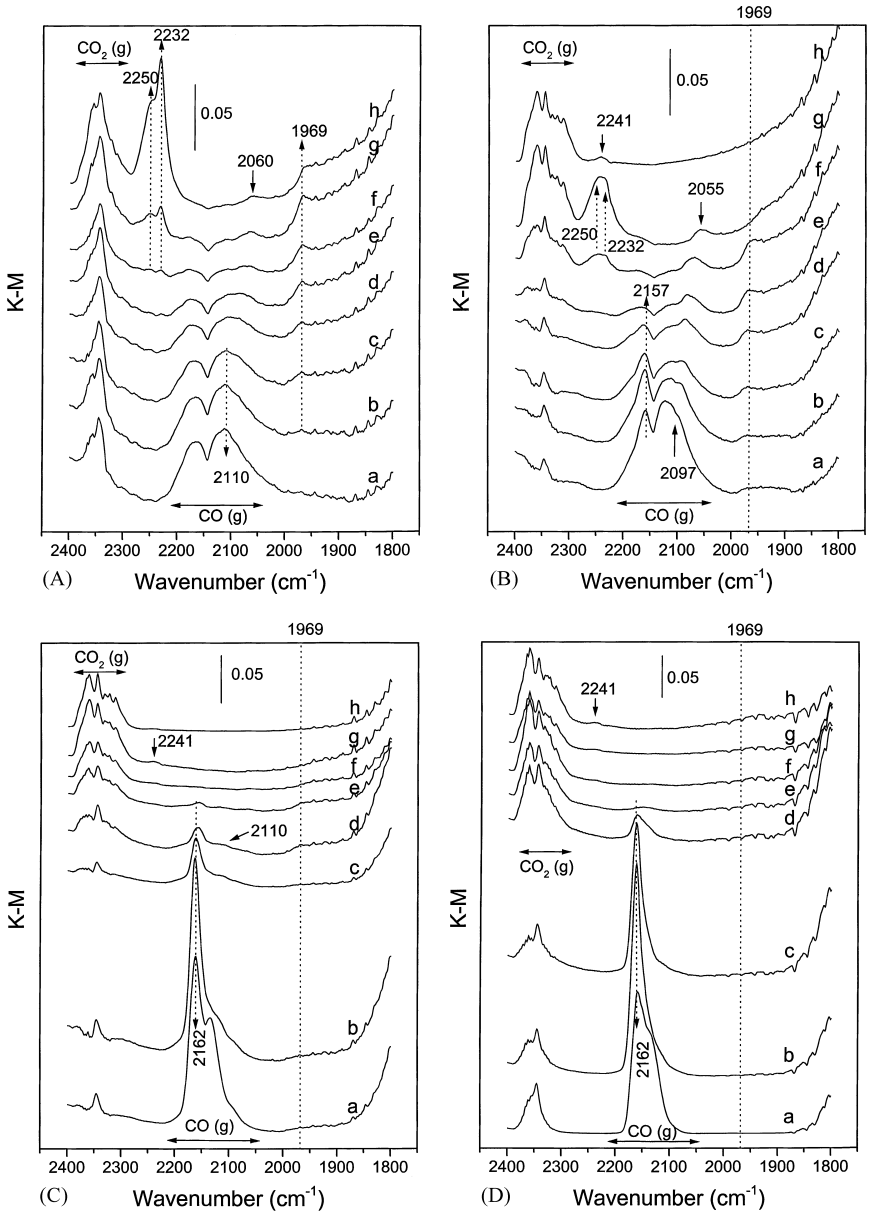

Fig. 2. (A) IR spectra of PdA sample in a flow of 1% CO, 0.45% O_2, 0.1% NO, N_2 balance at (a) 303, (b) 333, (c) 363, (d) 393, (e) 423, (f) 453, (g) 483, and (h) 513 K. (B) As Fig. 3A for Pd10ZCA. (C) As Fig. 3A for Pd33ZC. (D) As Fig. 3A for PdZC.

the onset of the NO dissociation. Interesting to note is that an alternative assignment to N_2O is not possible due to the absence of a band at ca. 1240 cm^{-1} [5,12]. Such NCO species are thus formed from NO dissociation at metallic sites and, following spillover, when adsorbed at exposed octahedral and tetrahedral Al^{3+} cations, yield frequencies of 2232 and 2250 cm^{-1} [10]. A weak band around 2240 cm^{-1}, which appears exclusively on ZC-containing catalysts, is assigned to NCO adsorption on ZC particles (Fig. 2Dh).

The changing state of Pd under reaction conditions can be followed by the appearance/disappearance of carbonyls indicative of adsorption on Pd(2+) (2162 cm^{-1}), Pd(+) (2110 cm^{-1}) and atop (2097 − 2060 cm^{-1}) and bridge (1970 cm^{-1}) Pd(0) sites [11,12]. Oxidized species seem to dominate the surface of the PdZC catalyst (Fig. 2D) which does not show evidence for the presence of metallic palladium. ZCA-supported samples evolve in a different manner. Pd33ZCA initially exposed only oxidized sites, although coexistence with metallic sites above 393 K was evident. The presence of metallic sites, in addition to the oxidized centers was evident from 303 K in the case of Pd10ZCA. For the PdA reference, an initial oxidized state of Pd, evidenced by a band at 2110 cm^{-1}, was present at the beginning of the reaction, coexisting with metallic sites (1969 cm^{-1}) from about 363 K. This is consistent with previous EPR experiments showing the presence of a Pd(+) signal when the sample was mildly reduced under CO [13]. In explaining the differences observed in detecting the metallic state, it must be recalled that population by the corresponding carbonyl species is subject to the availability of CO molecules in the gas phase; indeed, the disappearance of bridge sites upon increasing the temperature coincides approximately with the maximum in CO conversion (Fig. 1). On the other hand, the disappearance of Pd ion-bonded CO species may arise due to reduction to Pd(0), increased ease of desorption (due to weaker adsorption) at lower temperature than for bridged CO adsorbed on Pd(0) or/and by depletion of CO from the gas phase. Given that a certain relationship is observed between decreased intensity of these bands and increases in Pd(0) carbonyls, it seems that the main process contributing to removal of oxidized Pd-related carbonyls involved Pd reduction.

After running the $CO + NO + O_2$ reaction to 523 K and cooling to RT in nitrogen, IR spectra were obtained following CO admission (Fig. 3). Spectra show bands in the 2200–1800 cm^{-1} region indicative of the surface state of Pd at maximum conversion. Bands at 2099–2096 and 1993–1972 cm^{-1}, characteristic of CO adsorption on atop and bridge Pd(0) positions, respectively, dominate the spectra in all cases. The band due to the former was particularly week in the case of the PdA sample. An additional band, indicative of the presence of Pd(2+), and appearing at 2150 cm^{-1} for Pd*x*ZCA and 2130 cm^{-1} for PdZC, displayed increasing intensity with the ZC-content of the sample.

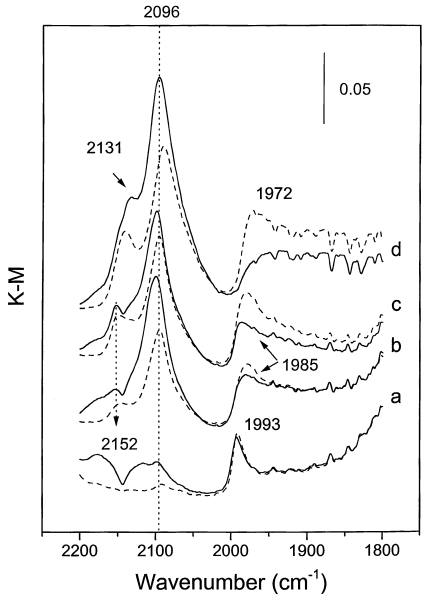

Fig. 3. IR spectra after CO admission at RT on used catalysts. (a) PdA; (b) Pd10ZCA; (c) Pd33ZCA; and (d) PdZC. Full line: 20 Torr; dashed line: after subsequent evacuation at 298 K.

3.3. XANES

The results of the Factorial Analysis for the Pd33ZCA Pd K-edge data, obtained during a temperature-programmed reaction run, are given in Table 1. Both the %SL and the reduced eigenvalues

Table 1
Pd K-edge principal factor analysis results

Number	Eigenvalue	%SL	*R*(*r*)	Variance[a]
1	374.73	0.00	482.31	99.968
2	0.07012	2.90	3.96	0.019
3	0.01583	19.80	1.68	0.004
4	0.00833	30.59	1.25	0.002
5	0.00584	36.25	0.97	0.002
6	0.00515	36.41	1.05	0.001
7	0.00411	39.05	0.95	0.001
8	0.00355	39.62	1.23	0.001
9	0.00226	48.92	0.81	
10	0.00206	51.51	0.79	

[a] Variances lower than 10^{-3} are not reported.

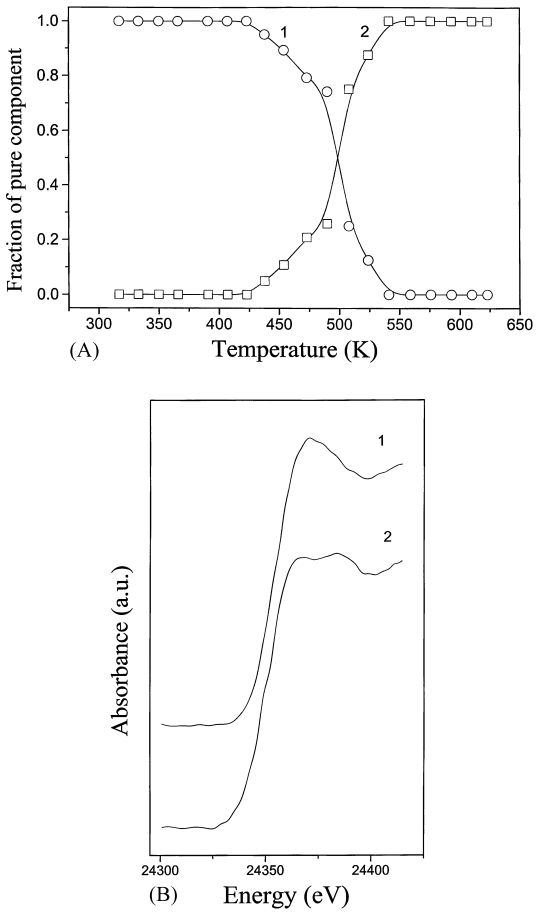

Fig. 4. (A) Evolution of individual components as a function of the reaction temperature in the XANES spectra at the Pd K edge. (B) Individual components obtained through analysis of Pd K edge XANES spectra.

conclusively show the existence of two distinguishable chemical species. Their concentration profiles through the reaction co-ordinate are displayed in Fig. 4A and their spectral shapes, as observed with the statistical analysis method, are displayed in Fig. 4B. These figures indicate the presence of an oxidized species which evolves from about 423 K yielding a reduced species with a maximum in the transformation rate at around 500 K. Comparison with XANES spectra of reference compounds [11] confirms that the two components (species 1 and 2) correspond to an oxidized species with local geometry similar to that of PdO (D_{2h} symmetry) and a reduced species with metal-like character. The latter when compared with the bulk state, presents a larger density of 5sp state (unusually high intensity of the continuum resonance at around 24360 eV, corresponding to the 1s $\rightarrow$ 5sp electronic transition), an effect which could be ascribed to the small particle size and/or electronic interactions with the ZC component of the support.

At the Ce L_{III}-edge, the XANES line-shape (data not shown) does not vary from that found for the calcined state when the sample is heated in the reactant gas atmosphere to 623 K. This means that the concentration of Ce^{3+} ions, if present, is below the detection limit, estimated at around 5% of the total Ce content.

3.4. EPR

Fig. 5 shows EPR spectra obtained after oxygen adsorption on samples which had been pretreated with CO and NO. According to results obtained by computer simulation, the spectra are formed by overlap of several signals, corresponding to different superoxide species stabilized by Ce cations (Table 2). All of the signals observed were the same as those detected after treatment under CO alone which were described

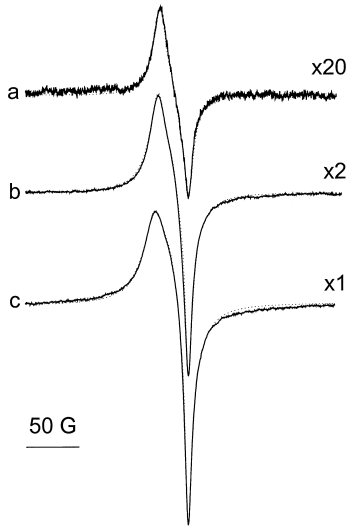

Fig. 5. EPR spectra (full lines) and computer simulation (overlapped dashed lines) following oxygen adsorption at 77 K on samples treated with CO (+vacuum) at 423 K and NO at 423 K. (a) Pd10ZCA; (b) Pd33ZCA; and (c) PdZC.

Table 2
Characteristics of the ESR signals observed after oxygen adsorption at 77 K on the samples treated under CO + NO at 423 K (see Section 2)

Signal	EPR parameters	Assignment	Intensity (μmol g$^{-1a,b}$)		
			Pd10ZCA	Pd33ZCA	PdZC
OCA1	$g_\perp = 2.027$, $g_{\|\|} = 2.012$	O_2^-–Ce^{4+} formed on 2D entities	0.13 (0.29)	1.24 (0.857)	
OCA2	$g_z = 2.027$–8, $g_x = 2.016$, $g_y = 2.011$				
OC1	$g_z = 2.031$, $g_x = 2.017$, $g_y = 2.011$	O_2^-–Ce^{4+} formed on isolated vacancies of 3D entities			2.87 (1.54)
OCPd[c]	$g_z = 2.032$–5, $g_x = 2.016$–7, $g_y = 2.012$	O_2^-–Ce^{4+} formed at Pd-ZC interfaces	0.005 (0.19)	0.55 (1.05)	2.45 (2.63)

[a] Evaluated by double integration of the spectra and comparison with a copper sulphate standard, and considering computer simulation results.
[b] The values in parentheses corresponds to the intensity observed after treatment under CO alone [1].
[c] As shown in Part 1 [1], the average width of this signal is considerably larger (27–31 G) than for the others (lower than ca. 9 G).

in Part 1 [1] of this study to which the reader is referred for details on their assignment.

The effect of NO treatment depends on the amount of Zr-Ce mixed oxide present in the catalyst (Table 2). The ratio (I_{CO+NO}/I_{CO}) between overall intensity of superoxide radicals detected upon O_2 adsorption after pretreatments in CO and NO and that found after pretreatment in CO only [1] increased with the amount of Zr–Ce mixed oxide. A large decrease was produced upon including a pretreatment in NO for Pd10ZCA whereas the same treatment for PdZC resulted in an increase in the relative number of superoxide radicals formed. This reflects that the main process resulting from NO interaction with the prereduced sample corresponds to oxidation of anion vacancies. This could proceed through NO adsorption on ZC surface vacancies, dimerization and further evolution of N_2O and/or N_2 [14], as well as by oxygen spillover from the palladium particles [15]. In terms of the amount of superoxide radicals formed in each case, this oxidative process leads to a hindering of superoxide formation for the sample with the lowest ZC content. For samples with higher ZC contents, it decreases the reducing power of the most reactive vacancies [1] favoring one-electron transfer processes (producing superoxide species) rather than the more reductive transfers involving two or more electrons per oxygen molecule (producing diamagnetic peroxide or oxide species). Analysis of the relative intensities of the signals (Table 2) shows that the centers which are most affected by this oxidative process are those located close to Pd-promoter interfaces (signal OCPd).

4. Discussion

Analysis of the reactivity profiles (Fig. 1) reveals that the promoting effect of ZC is different for CO oxidation and NO reduction reactions. While CO oxidation activity increases with the amount of mixed oxide, the greatest promoting effect for NO reduction is achieved, both in terms of NO conversion and N_2 selectivity, over Pd33ZCA.

Comparison between CO conversion profiles in the absence [1] and in the presence of NO (Fig. 1) reveals that NO has an inhibiting effect on the CO oxidation activity. The isoconversion temperatures for CO oxidation over PdA, were ca. 30 K higher in the presence of NO, although the presence of NO could hinder Pd reduction at low temperatures for this catalyst, as indicated by the presence of a Pd^+ band at 2110 cm^{-1} from 303 K which is absent when similar experiments were performed in the absence of NO [1,13]. DRIFTS experiments (Fig. 2A) show that the active Pd metallic state is achieved well before the onset of CO oxidation. This suggests that the situation is similar to that observed in the absence of NO. The reaction is limited by the rate of CO desorption from metallic Pd surfaces which are nearly CO-saturated because at temperatures below the onset of reaction, the strongly adsorbed CO hinders adsorption-dissociation of the other reactants (O_2 and/or NO). This is consistent with the presence of bridging carbonyls (1969 cm^{-1}) for $T \leq 483$ K, the band intensity of which decreases only at higher temperature, while showing a red shift, indicative of a decrease in CO coverage [16]. The

presence of atop carbonyls at 2082 cm^{-1} for $T \leq$ 453 K also suggests that a relatively high CO coverage of the Pd surface is maintained at those temperatures. The lower activity for CO oxidation observed in the presence of NO can therefore be attributed to a smaller O coverage over the Pd particles, resulting from competition between NO and O_2 for the metallic adsorption sites. This is consistent, with the temperature of formation of isocyanate species (NCO) on the alumina surface, which results from interaction between CO and N species co-adsorbed on the metallic Pd surface followed by spillover to the alumina surface [17] which is indicative of the onset of the N–O dissociation.

An inhibiting effect of the presence of NO on CO oxidation activity was also observed for the ZC-containing catalysts. Comparison of these catalysts (Fig. 1 and ref. [1]) shows that PdZC was the most affected by this interaction as the temperature for 100% conversion was decreased by ca. 100 K. In contrast, Pd10ZCA shows only a ca. 30 K lower isoconversion temperatures while Pd33ZCA is almost unaffected by the presence of NO, showing only a slightly lower activity for temperatures below 350 K. Assuming that active sites for CO oxidation are similar in all these catalysts, namely sites at which contact exists between Pd and aggregated 3D-ZC entities [1], the modifying effects produced by the presence of NO in the reactant mixture suggest that different deactivation mechanisms are involved in each of these systems as a function of the reaction temperature at which the systems are active for CO oxidation and/or of the kind of Pd entity present at each reaction temperature. At relatively low temperatures, DRIFTS results (Fig. 2 and data Fig. 5 in Part 1 [1]) show that the presence of NO induces the formation of oxidized Pd states in all catalysts, as indicated by the presence of bands at 2162–2110 cm^{-1} whose relative intensity increases with ZC content. As characterization results [1,18] indicate that the amount of aggregated 3D-ZC entities increases with ZC concentration, it can be concluded that formation of these oxidized Pd states is characteristic of interactions between Pd and 3D-ZC entities. This suggests in turn that Pd-3D-ZC interface sites which would be reduced by CO at low temperatures are readily oxidized upon contact with NO, passivating the active sites as a result of this interaction. Evidence for this NO-induced interface oxidation process is provided by EPR experiments (Fig. 5 and Table 2). The extent of this deactivating oxidation process decreases with increasing reaction temperature, as indicated by the extent to which the intensity of the bands at 2162–2110 cm^{-1} at 333–363 K is decreased (Fig. 2). This oxidation might explain the large low temperature deactivation of the most active CO oxidation catalyst (PdZC), while the alumina-supported catalysts, which are active only at higher temperatures, are less affected. Differences between Pd10ZCA and Pd33ZCA in terms of CO oxidation activity in the presence of NO are of moderate magnitude. DRIFTS results indicate the more facile generation of metallic Pd for Pd10ZCA, as indicated by the greater overall intensity of bridge and atop carbonyls (bands at ca. 1970 and 2097–2055 cm^{-1}, respectively) adsorbed at Pd^0 sites. This can be rationalized by comparing DRIFTS results with the PdA sample. Pd particles in contact with alumina are apparently readily reduced but O_2 activation is only achieved at high temperature. Observed differences between PdxCA samples can be ascribed to the fraction of Pd in contact with the ZC-component, which is maximized for Pd33ZCA. On the other hand, differences in the Pd particle size or morphology which could induce differences in the CO/NO competitive adsorption process [20] are not expected in view of the similar initial (Fig. 2) and final (Fig. 3) state of Pd in ZC-containing materials.

NO reduction profiles indicate differences between the catalysts in the extent to which ZC promotes the reaction, which must be attributed to the different nature and physico-chemical properties of the ZC entities present and influencing the Pd species in each case. Again, the NO reduction process may also depend on the Pd particle size and morphology, due to the structure sensitivity of the N-O dissociation process [21], but these characteristics appear to be very similar for all the ZC-based systems (Fig. 3). Therefore, the NO reduction characteristics, in terms of both conversion and N_2 selectivity, must be attributed to the specific properties of Pd-ZC contacts present in each case. The greater activity of ZCA-supported samples and, among these, of the Pd33ZCA catalyst, suggests that the ZC entities involved in this promoting effect may correspond to small 3D-ZC particles or highly dispersed 2D-ZC species, interacting directly with the alumina surface, which both appear in increasing amounts as

the ZC loading is increased in the alumina-supported samples [1,18]. Previous studies [18,19] have shown that both entities present different redox properties, and also properties which differ from those exhibited by unsupported ZC. These differences were attributed to the influence of alumina on the growth of the ZC particles (for 3D-ZC) or to a direct modification of the immediate chemical environment of the Ce and Zr ions in them (for 2D-ZC). It would be relevant therefore to clarify to what extent, and in which way, such differences might be responsible for the differences observed in catalytic activity. EPR results (Fig. 5and Table 2) are not conclusive in this respect since, as shown for Pd10ZCA, both kinds of entities may be involved in NO activation, as a significant hindering of superoxide formation, attributed to oxidation of anionic vacancies, is produced for both entities upon NO treatment. Nevertheless, it should be noted that 2D-ZC entities are easier to reduce than 3D-ZC or unsupported ZC, while the oxygen vacancies created on them are the most difficult to oxidize by both NO and O_2. This suggests that a Pd reduced state, which is the most active for NO dissociation [2,4], would be more easily achieved in the presence of Pd interactions with those supposedly more reduced 2D-ZC species, at least under the present reaction conditions in which contact between palladium and 3D-ZC entities seems to favor formation of oxidized states of Pd (Figs. 2 and 3). In fact, the onset of NO reduction coincides approximately with generation of metallic Pd, as indicated by both DRIFTS and XANES experiments (Figs. 2 and 4), indicating that activation of NO proceeds through interaction with fully metallic Pd particles, in agreement with previous work [2,4]. However, this cannot be the main factor in determining catalytic activity since the Pd33ZCA catalyst is the most active. The relatively facile reaction of Pd-adsorbed NO with ZC-based anion vacancies, as indicated by EPR (Fig. 5), could be significant. Such reaction might lead to N–O bond breaking with the O-fragment filling the anion vacancy and the N adatom forming a nitride-like species on Pd (which from the position of carbonyl IR bands would appear as oxidized Pd). A similar mechanism (enhancement of O–O bond breaking at the interface) may also apply to the CO/O_2 reaction. The fact that the catalyst which displays maximal ZC promotion for NO conversion is not the same as the catalysts giving maximum enhancement for CO conversion suggests that these effects (enhancement of the Pd reduced state and enhancement of bond breaking at the interface), which are of different magnitudes for the different types of ZC entities, have different relative importance for each of the reactions involved. Although no definitive conclusion can be established, this distinct promotion of CO oxidation and NO reduction reactions among the examined catalysts can be due to operation of different kinds of centers for each reaction. This suggests that centers which are most efficient for NO reduction may correspond to interactions between Pd and 2D-ZC entities. This hypothesis correlates well with results for similar catalysts using ceria, instead of ZC, as promoter [22]. In that case, the greater promoting effect on NO reduction under similar reaction conditions on comparing Pd supported on ceria/alumina samples was also observed over the sample showing the greater amount of two-dimensional ceria species.

5. Conclusions

A series of palladium catalysts supported on ceria–zirconia, ceria–zirconia/alumina and alumina has been studied by means of catalytic activity tests, and by DRIFTS, XANES and EPR spectroscopies, with regard to their light-off behavior for CO oxidation and NO reduction under stoichiometric $CO + NO + O_2$ gas mixtures. A promoting effect of the Zr-Ce mixed oxide on both reactions is observed. The extent of promotion depends on the characteristics of the promoter entities present for each catalyst and on the nature of the reaction. CO oxidation activity is mainly enhanced by contact between Pd and 3-D aggregated promoter entities as evidenced by correlation between characterization [1] and catalytic results showing increasing activity with increasing Zr-Ce mixed oxide content. At low temperature, an inhibiting effect of NO on CO oxidation, attributed to passivation of the interface sites due to formation of oxidized states of Pd (evidenced by DRIFTS), produces certain lower CO oxidation activity than in the absence of NO [1]. On the contrary, the higher activity for NO reduction is exhibited by catalysts supported on ceria–zirconia/alumina. This suggests that most active sites for that reaction involve Pd interacting with highly dispersed zirconia-ceria entities, most likely in the form of 2D-patches. Two different effects

(enhancement of the Pd reduced state and enhancement of N–O bond breaking at the interface between Pd and Zr–Ce mixed oxide entities), with the latter having a higher relative importance, are proposed to be involved in the NO reduction activity promotion.

Acknowledgements

A. M.-A. gratefully acknowledges the "Comunidad de Madrid" for a Postdoctoral grant and for financial help under the "Ayudas para estancias breves en centros de investigación extranjeros" program. A. I.-J. also thanks the "Comunidad de Madrid" for a Predoctoral grant. Support from CAICYT (Project No. MAT 97-0696-CO2-O1) and CAM (Project No. 06M/084/96) is fully appreciated. Thanks are due to the scientific staff of the EXAFS IV line at LURE for their help during XANES measurements.

References

[1] M. Fernández-García, A. Martínez-Arias, A. Iglesias-Juez, A.B. Hungría, J.A. Anderson, J.C. Conesa, J. Soria, Appl. Catal. B. 31 (2001) 39.
[2] M. Fernández-García, A. Martínez-Arias, C. Belver, J.A. Anderson, J.C. Conesa, J. Soria, J. Catal. 190 (2000) 387.
[3] R.J. Farrauto, R.M. Heck, Catal. Today 51 (1999) 351.
[4] M. Fernández-García, A. Martínez-Arias, J.A. Anderson, J.C. Conesa, J. Soria, Stud. Surf. Sci. Catal. 130 (2000) 1325.
[5] R. Di Monte, P. Fornasiero, J. Kaspar, P. Rumori, G. Gubitosa, M. Graziani, Appl. Catal. B. 24 (2000) 157.
[6] R.A. Searles, Stud. Surf. Sci. Catal. 116 (1998) 23.
[7] M. Fernández-García, C. Márquez-Alvarez, G.L. Haller, J. Phys. Chem. 99 (1995) 12565.
[8] C. Márquez-Alvarez, I. Rodríguez-Ramos, A. Guerrero-Ruiz, G.L. Haller, M. Fernández-García, J. Am. Chem. Soc. 119 (1997) 2905.
[9] E.R. Malinowsky, Factor Analysis in Chemistry, Wiley, New York, 1991.
[10] J.A. Anderson, C. Márquez-Alvarez, M.J. López-Muñoz, I. Rodríguez-Ramos, A. Guerrero-Ruiz, Appl. Catal. B 14 (1997) 189.
[11] M. Fernández-García, J.A. Anderson, G.L. Haller, J. Phys. Chem. 100 (1996) 16247.
[12] A. Bensalem, J.C. Muller, D. Tessier, F. Bozon-Verduraz, J. Chem. Soc., Faraday Trans. 92 (1996) 3233.
[13] M. Fernández-García, A. Martínez-Arias, L.N. Salamanca, J.M. Coronado, J.A. Anderson, J.C. Conesa, J. Soria, J. Catal. 187 (1999) 474.
[14] A. Martínez-Arias, J. Soria, J.C. Conesa, X.L. Seoane, A. Arcoya, R. Cataluña, J. Chem. Soc., Faraday Trans. 91 (1995) 1679.
[15] A. Trovarelli, Catal. Rev. Sci. Eng. 38 (1996) 439.
[16] X. Xu, D.W. Goodman, J. Phys. Chem. 97 (1993) 7711.
[17] K. Almusaiteer, S.S.C. Chuang, J. Catal. 184 (1999) 189.
[18] M. Fernández-García, A. Martínez-Arias, A. Iglesias-Juez, C. Belver, A.B. Hungría, J.C. Conesa, J. Soria, J. Catal. 194 (2000) 385.
[19] A. Martínez-Arias, M. Fernández-García, C. Belver, J.C. Conesa, J. Soria, Catal. Lett. 65 (2000) 197.
[20] X. Xu, P. Chen, D.W. Goodman, J. Phys. Chem. 98 (1994) 9242.
[21] X. Xu, D.W. Goodman, Catal. Lett. 24 (1994) 31.
[22] A. Martínez-Arias (unpublished results).